

Revisit of series-SSHI with comparisons to other interfacing circuits in piezoelectric energy harvesting

This article has been downloaded from IOPscience. Please scroll down to see the full text article.

2010 Smart Mater. Struct. 19 125009

(<http://iopscience.iop.org/0964-1726/19/12/125009>)

View [the table of contents for this issue](#), or go to the [journal homepage](#) for more

Download details:

IP Address: 111.240.226.181

The article was downloaded on 23/10/2010 at 02:19

Please note that [terms and conditions apply](#).

Revisit of series-SSHI with comparisons to other interfacing circuits in piezoelectric energy harvesting

I C Lien¹, Y C Shu^{1,3}, W J Wu², S M Shiu¹ and H C Lin¹

¹ Institute of Applied Mechanics, National Taiwan University, Taipei 106, Taiwan, Republic of China

² Department of Engineering Science and Ocean Engineering, National Taiwan University, Taipei 106, Taiwan, Republic of China

E-mail: yichung@iam.ntu.edu.tw

Received 11 June 2010, in final form 20 September 2010

Published 22 October 2010

Online at stacks.iop.org/SMS/19/125009

Abstract

SSHI (synchronized switch harvesting on inductor) techniques have been demonstrated to be capable of boosting power in vibration-based piezoelectric energy harvesters. However, the effect of frequency deviation from resonance on the electrical response of an SSHI system has not been taken into account from the original analysis. Here an improved analysis accounting for such an effect is proposed to investigate the electrical behavior of a series-SSHI system. The analytic expression of harvested power is proposed and validated numerically. Its performance evaluation is carried out and compared with the piezoelectric systems using either the standard or parallel-SSHI electronic interfaces. The result shows that the electrical response of an ideal series-SSHI system is in sharp contrast to that of an ideal parallel-SSHI system. The former is similar to a strongly coupled electromechanical standard system operated at the open circuit resonance, while the latter is analogous to that operated at the short circuit resonance with different magnitudes of matching impedance. In addition, the performance degradation due to non-ideal voltage inversion is also discussed. It shows that a series-SSHI system avails against the standard technique in the case of medium coupling, since its peak power is close to the ideal optimal power and the reduction in power is less sensitive to frequency deviation. However, the consideration of inevitable diode loss in practical devices favors the parallel-SSHI technique, since the frequency-insensitive feature is much more pronounced in parallel-SSHI systems than in series-SSHI systems.

(Some figures in this article are in colour only in the electronic version)

1. Introduction

Power harvesting refers to energy retraction from ambient surroundings and converting it into useful electric energy. With advances in wireless technology and low-power electronics, energy harvesting from environmental resources has the potential to power mobile and wireless microsystems where battery replacement is either practically impossible or prohibitively expensive [7, 26, 31, 48]. Due to the ubiquitous presence of ambient vibrations, extensive research efforts have been made for converting mechanical energy into

electrical power through piezoelectric, electromagnetic and capacitive transducers [36, 40]. Amongst them, piezoelectric vibration-to-electricity converters have been viewed as being superior to other means, as they have high electromechanical coupling, no external voltage source requirement and they are particularly attractive for use in MEMS [15, 20, 40] and nanosystems [28, 38]. As a result, the use of piezoelectric materials for scavenging energy from ambient vibration sources has recently witnessed a dramatic rise for power harvesting [5, 13, 24, 25, 49, 56].

A vibration-based piezoelectric energy harvesting system includes three essential components: an oscillator, a

³ Author to whom any correspondence should be addressed.

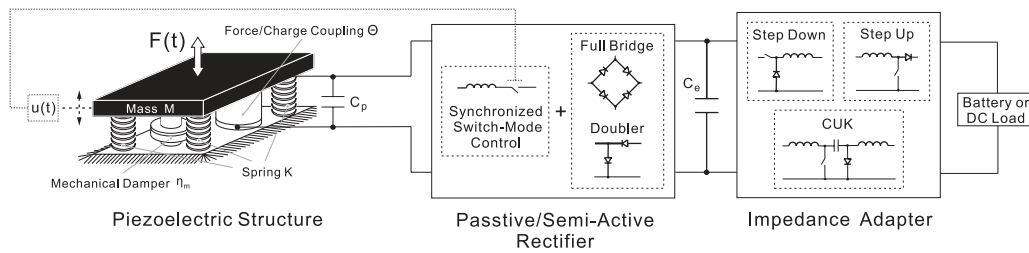


Figure 1. An equivalent model representing a vibration-based piezoelectric energy harvesting system.

piezoelectric medium and an energy storage circuit, as demonstrated in figure 1. An oscillator is designed to transmit ambient vibrations into mechanical strain energy which is converted into electrical energy via the direct piezoelectric effect. The generated charges are accumulated through an interfacing circuit for AC/DC conversion and presented to a load circuit. Precisely, the power generator is typically designed as a resonant oscillator since the peak power is achieved when the driving frequency matches the device's resonance [40]. The transducer materials for energy conversion include PZT, PVDF and the newly emerged ferroelectric relaxors such as PMN-PT [30, 50]. They have been used in various types of structures to serve specific purposes, such as cantilever beams in transverse excitation bases [1, 16, 35] and plates (diaphragms) in pressure-loaded environments [17, 32]. The layout of electrodes on the plate's surfaces has to be carefully patterned to avoid charge cancellation [18, 41]. The design of generators based on non-resonant excitations has also received considerable recent attention [3, 37, 42, 52].

The circuit design is required for electrical compatibility and maximum power transfer to the load. It consists of AC/DC interfacing electronics connecting the piezoelectric element to the terminal electric load. Power optimization schemes therefore depend not only on the mechanical solicitation, but also on the specific types of interfacing circuits. This motivates a variety of research efforts for proposing appropriate electronic interfaces. The most common one is the standard interface which includes an AC/DC rectifier followed by a filtering capacitance, as shown in the middle of figure 1. Ottman *et al* [33] have studied the electrical behavior of this standard system based on the uncoupled model which simplifies the vibrating piezoelectric structure as the current source in parallel with its internal capacitance. They further developed adaptive DC/DC converters for impedance matching [34]. Shu and Lien [44] subsequently proposed an improved analysis for optimizing AC/DC power extraction without the uncoupled assumption. They also investigated the relation between electrically induced damping and conversion efficiency for a rectified piezoelectric device [45] (cf [22, 23, 39]). The result shows that optimization criteria vary according to the relative strength of electromechanical coupling to mechanical damping ratio. Guan and Liao [10, 11] analyzed the charge/discharge efficiencies for several different energy storage devices. Wu *et al* [54] and Wickenheiser *et al* [53] investigated the transient behavior of a storage capacitor under charging. Liu *et al* [27] used the switch-mode power electronics to develop a scheme for active energy harvesting.

Based on the beam model, Hu *et al* [14] numerically studied the interaction between the piezoelectric vibrating structure and the storage circuit.

Another recently emerged energy harvesting circuit is the 'synchronized switch harvesting on inductor' (SSHI) interface which is added to the piezoelectric element together with the standard DC technique, as also illustrated in the middle of figure 1. This technique was proposed by Guyomar and his co-workers [2, 12, 19, 21, 29] who have shown that power is boosted significantly in a weakly coupled electromechanical system. However, the effect of frequency deviation from resonance on the electrical behavior of an SSHI system is not taken into account in the original analysis. Instead, Shu *et al* [46] have proposed several improved estimates for the parallel-SSHI circuit accounting for this effect. They have shown that the electrical response of a parallel-SSHI system is similar to that of a strongly coupled electromechanical standard system operated at the short circuit resonance. Furthermore, this technique improves the scavenger's bandwidth significantly in comparison to the standard technique. Here, we provide another improved analysis for electrical performance evaluation of a series-SSHI system. It takes into account the full electromechanical coupling response and vibration phase-shift effect, and therefore the analysis is capable of revealing the system characteristics in the vicinity of resonance. The results show that the electrical behaviors of these two ideal SSHI systems are conjugate with each other in comparison to the standard technique. However, they exhibit a dissimilar response if the effect of diode loss is considered. It turns out the feature of wideband could be lost in practical devices endowed with series-SSHI circuits. Finally, some of our preliminary results have been reported in a conference paper [47]. Here, we systematically derive the main results with numerical validation and provide discussions concerning electrical loss in detail.

This paper is organized as follows. First a piezoelectric transducer is modeled as a lumped single-degree-of-freedom system undergoing periodic forcing in section 2. A number of research efforts based on the distributed parameter methods have been made for analyzing a vibrating piezoelectric structure connected to a single resistor [4, 8, 9, 16, 43]. They show advantages in predicting the model shapes, strain distribution and energy harvesting performance based on geometry and material properties of a structure. However, difficulties arise if the nonlinear interfacing circuits are taken into account in analysis [14]. Limited success has been achieved by bridging structural modeling and circuit

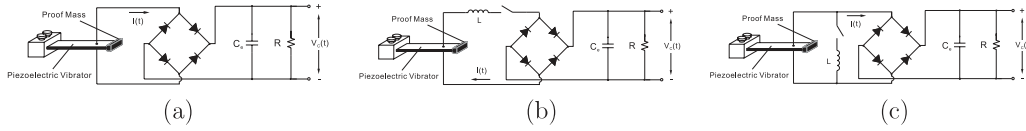


Figure 2. (a) A standard harvesting circuit. (b) A series-SSHI harvesting circuit. (c) A parallel-SSHI harvesting circuit.

simulation such as coupled FEM–SPICE models [6, 55]. Hence, if the focus is the overall electrical behavior rather than the detailed response at each specific point of a structure, the reduced model suffices the need for harvesting circuit design. Subsequently, an energy harvester using the standard circuit is introduced in section 2.1 and the electrical response of a series-SSHI system is analyzed in detail in section 2.2. The harvested power is derived and expressed explicitly in terms of several dimensionless system parameters. The operating points for achieving optimal power is also discussed there. For the purpose of comparison, the electrical behavior of a parallel-SSHI system is briefly reviewed in section 2.3. Next, the results are numerically validated in section 3.1 and are discussed under the case of non-ideal voltage inversion in section 3.2 and the case of diode loss in section 3.3. The conclusions are made in section 4.

2. Energy harvesting interfacing circuits

Consider a piezoelectric structure whose modal density is assumed to be widely separated. Suppose it is vibrating at around its resonance frequency. In this case, the resonator is modeled as a mass + spring + damper + piezo structure shown in figure 1. It consists of a piezoelectric element coupled to a mechanical structure with governing equations described by [44]

$$M\ddot{u}(t) + \eta_m \dot{u}(t) + Ku(t) + \Theta V_p(t) = F(t), \quad (1)$$

$$-\Theta \dot{u}(t) + C_p \dot{V}_p(t) = -I(t), \quad (2)$$

where u is the displacement of the mass M , V_p the voltage across the piezoelectric element, $F(t)$ the forcing function applied to the system and $I(t)$ the current flowing into the specified circuit. In addition, in equations (1) and (2), η_m is the mechanical damping coefficient, K is the stiffness of the structure, Θ is the piezoelectric coefficient and C_p is the clamped capacitance. The explicit expressions of these effective coefficients depending on the material constants and the design of harvesters can be obtained using the standard modal analysis [51]. In addition, most applications of piezoelectric materials for power generation involve the use of periodic straining of piezoelectric elements. Thus, the excitation considered here is assumed to be harmonic with

$$F(t) = F_0 \sin \omega t, \quad (3)$$

where F_0 is the constant magnitude and ω (in radians per second) is the angular frequency of vibration.

Besides the piezoelectric structure designed for transmitting and converting ambient vibrations to electrical energy, it is imperative to include a suitable circuit system for charge

storage, as also shown in figure 1. First, the electric compatibility has to be guaranteed since a vibrating piezoelectric element generates an AC voltage rather than DC output. To achieve this goal, a rectifier followed by a filtering capacitance C_e is added for AC/DC conversion. Next, an adapter between the rectifier output and the battery is included for impedance matching. Typically, the analysis is simplified by replacing the regulation circuit and battery with an equivalent resistor R as shown in figure 2(a), where V_c is the rectified voltage across the electrical load. It therefore comprises a standard energy harvesting circuit commonly used for design analysis. In addition to the passive rectifier, certain semi-active rectifying techniques have also been proposed recently for power boosting, as schematically shown in the middle of figure 1. It consists of a synchronized switch-mode control for piezoelectric voltage inversion by monitoring system displacement. Examples including the series and parallel-SSHI techniques are illustrated in figures 2(b) and (c) [2, 12, 21]. Since the electrical behavior is significantly influenced by the electronic interface connecting the piezoelectric element and terminal load, these distinct harvesting circuits are analyzed now.

2.1. Standard interface

Consider the case of a standard circuit shown in figure 2(a). Typically, the filter capacitor C_e is chosen to be large enough so that the rectified voltage V_c is essentially constant to have a stable DC output voltage [33]. Besides, the rectifying bridge used here is assumed to be perfect so that it is open circuited if the piezoelectric voltage $|V_p| < V_c$. As a result, the current flowing into the circuit vanishes. On the other hand, when $|V_p|$ reaches V_c , the bridge conducts and the piezoelectric voltage is kept equal to the rectified voltage, i.e. $|V_p| = V_c$. Finally, the conduction in the rectifier diodes is blocked again when $|V_p(t)|$ starts decreasing. The typical waveforms of $u(t)$ and $V_p(t)$ are schematically illustrated in figure 3(a) under the harmonic excitation of a single signal.

The steady-state response of the piezoelectric system has been studied by various approximations such as uncoupled and in-phase models. The former models the piezoelectric device as the current source in parallel with its internal capacitance C_p [33], while the latter assumes that the external forcing function and the velocity of the mass are in-phase [12]. An improved analysis accounting for the full electromechanical behavior of the system and the phase-shift effect has been proposed by Shu and Lien [44, 45]. They showed that the displacement magnitude u_0^{Standard} , rectified voltage V_c^{Standard} and harvested average power P^{Standard} can be expressed in terms of several dimensionless variables by (see

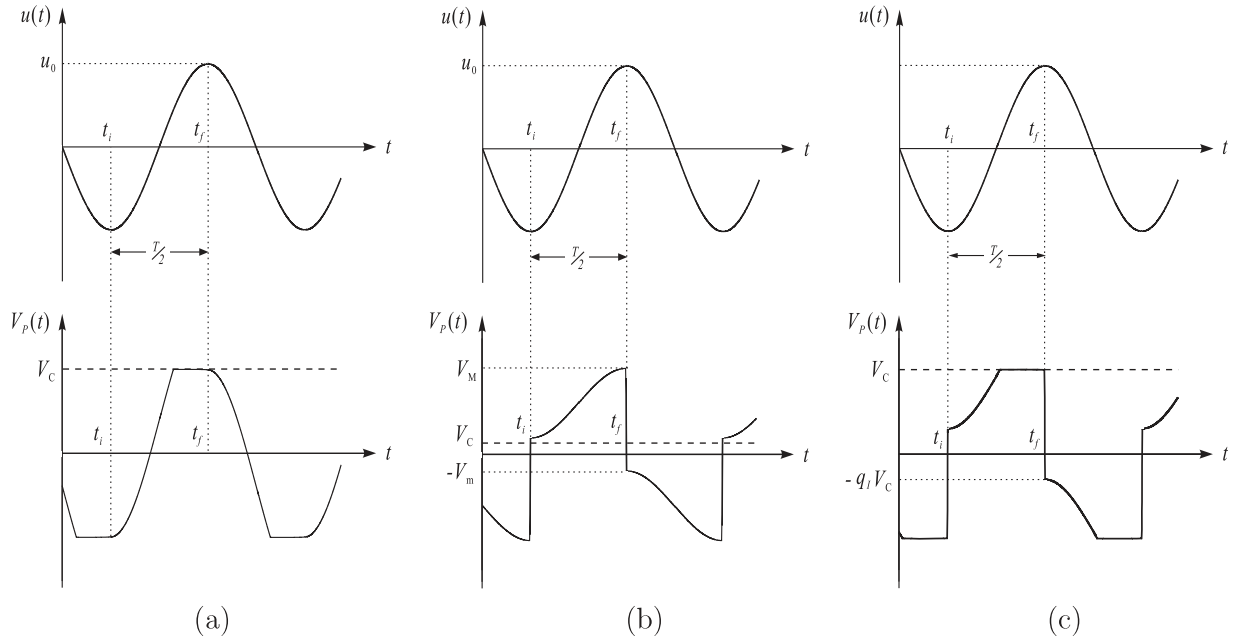


Figure 3. Typical waveforms of displacement and piezoelectric voltage for (a) the standard interface, for (b) the series-SSHI interface and (c) the parallel-SSHI interface.

equations (28)–(30) in [44])

$$\bar{u}_0^{\text{Standard}} = \frac{u_0^{\text{Standard}}}{\frac{F_0}{K}} = \frac{1}{\left\{ \left(2\zeta_m + \frac{2k_e^2 r}{(r\Omega + \frac{\pi}{2})^2} \right)^2 \Omega^2 + \left(1 - \Omega^2 + \frac{k_e^2 r \Omega}{r\Omega + \frac{\pi}{2}} \right)^2 \right\}^{\frac{1}{2}}}, \quad (4)$$

$$\bar{V}_c^{\text{Standard}} = \frac{V_c^{\text{Standard}}}{\frac{F_0}{\Theta}} = \left(\frac{r\Omega}{r\Omega + \frac{\pi}{2}} \right) \times \frac{k_e^2}{\left\{ \left(2\zeta_m + \frac{2k_e^2 r}{(r\Omega + \frac{\pi}{2})^2} \right)^2 \Omega^2 + \left(1 - \Omega^2 + \frac{k_e^2 r \Omega}{r\Omega + \frac{\pi}{2}} \right)^2 \right\}^{\frac{1}{2}}}, \quad (5)$$

$$\bar{P}^{\text{Standard}} = \frac{P^{\text{Standard}}}{\frac{F_0^2}{w_{sc} M}} = \frac{1}{(r\Omega + \frac{\pi}{2})^2} \times \frac{k_e^2 \Omega^2 r}{\left\{ \left(2\zeta_m + \frac{2k_e^2 r}{(r\Omega + \frac{\pi}{2})^2} \right)^2 \Omega^2 + \left(1 - \Omega^2 + \frac{k_e^2 r \Omega}{r\Omega + \frac{\pi}{2}} \right)^2 \right\}}, \quad (6)$$

where $\bar{u}_0^{\text{Standard}}$, $\bar{V}_c^{\text{Standard}}$ and $\bar{P}^{\text{Standard}}$ are normalized displacement, voltage and power, and

$$k_e^2 = \frac{\Theta^2}{K C_p}, \quad \zeta_m = \frac{\eta_m}{2\sqrt{KM}}, \quad w_{sc} = \sqrt{\frac{K}{M}}, \quad (7)$$

$$\Omega = \frac{w}{w_{sc}}, \quad r = C_p w_{sc} R.$$

Above, k_e^2 is the alternative electromechanical coupling coefficient, ζ_m the mechanical damping ratio, w_{sc} the natural frequency of the short circuit, and Ω and r the normalized frequency and electrical resistance [5, 24, 25, 35]. Notice that there are two resonances for the system since the piezoelectric structure exhibits both short circuit and open circuit stiffness. Let Ω_{sc} and Ω_{oc} be the frequency ratios of short circuit and

open circuit. They are defined by

$$\Omega_{sc} = 1, \quad \Omega_{oc} = \sqrt{1 + k_e^2}. \quad (8)$$

An important feature from this improved analysis is that the electrical behavior of the piezoelectric system is significantly influenced by the ratio of electromechanical coupling factor to mechanical damping ratio, i.e. $\frac{k_e^2}{\zeta_m}$. Harvested power is small if this ratio is much smaller than one, while it achieves a saturation value if this ratio is much larger than one. Indeed, if the shift in device natural frequency is pronounced or the mechanical damping ratio of the system is small, i.e. $\frac{k_e^2}{\zeta_m} \gg 1$, there are two optimal operating points. The first optimal pair is designed at the short circuit resonance Ω_{sc} with the optimal load $r_{sc}^{\text{opt}} \propto \frac{1}{\frac{k_e^2}{\zeta_m}}$ (equation (49) in [44]), while the second one is designed at the open circuit resonance Ω_{oc} with the optimal load $r_{oc}^{\text{opt}} \propto \frac{1}{(1+k_e^2)\frac{k_e^2}{\zeta_m}}$ (equation (55) in [44]). Both gives the identical value of maximum harvested power which depends only on the damping ratio ζ_m and is independent of the coupling coefficient k_e^2 . Indeed, the dependence of average DC power on the electrical load and applied frequency is schematically shown in figure 4(a) for a strongly coupled electromechanical standard system ($k_e^2 = 1.0$, $\zeta_m = 0.03$, $\frac{k_e^2}{\zeta_m} = 33$). It is clear that there are two identical peaks evaluated at around these two optimal pairs ($\Omega_{sc}, r_{sc}^{\text{opt}}$) and ($\Omega_{oc}, r_{oc}^{\text{opt}}$). Finally, table 1 summarizes the relation between the system parameters (k_e^2, ζ_m) and the normalized load, displacement, voltage, current and power at these two optimal conditions [44]. This table will be used later to identify the electrical response of series- and parallel-SSHI systems which are shown to be closely related to the strongly coupled electromechanical system using the standard interface.

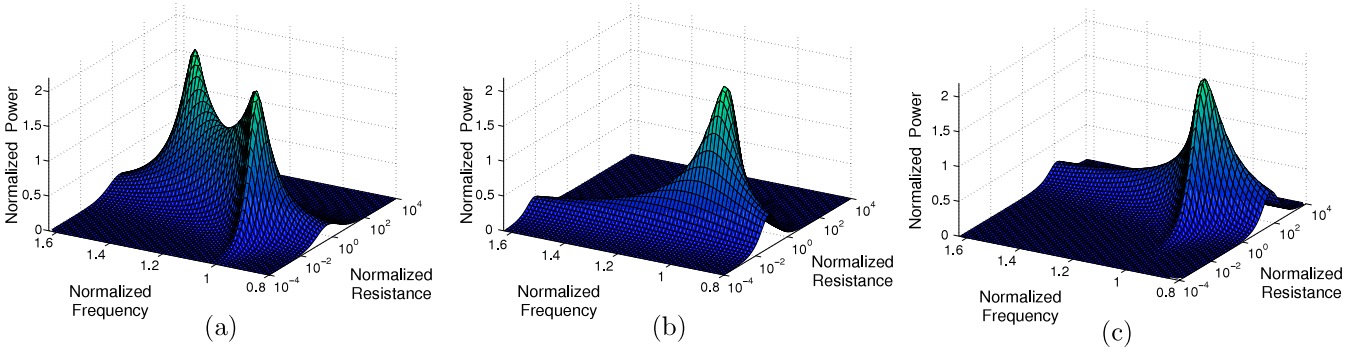


Figure 4. The harvested DC power against the electrical resistance and applied frequency for standard (equation (6)), series-SSHI (equation (21)) and parallel-SSHI (equation (26)) techniques. (a) A standard system with strong electromechanical coupling ($k_e^2 = 1.0$, $\zeta_m = 0.03$, $\frac{k_e^2}{\zeta_m} = 33$). (b) An ideal series-SSHI system with weak electromechanical coupling ($k_e^2 = 0.01$, $\zeta_m = 0.03$, $\frac{k_e^2}{\zeta_m} = 0.33$, $Q_1 = \infty$). (c) An ideal parallel-SSHI system with weakly electromechanical coupling ($k_e^2 = 0.01$, $\zeta_m = 0.03$, $\frac{k_e^2}{\zeta_m} = 0.33$, $Q_1 = \infty$). Notice that the magnitudes of peak power are identical in these three cases, but they are achieved at different operating conditions and system parameters.

Table 1. There are two optimal operating points (Ω_{sc} , r_{sc}^{opt}) and (Ω_{oc} , r_{oc}^{opt}) in a strongly coupled electromechanical standard system ($\frac{k_e^2}{\zeta_m} \gg 1$). The dependence of optimal displacement, voltage, current and power on the system parameters k_e^2 and ζ_m are provided at these two optimal pairs. It is shown later that the behavior of parallel-SSHI is similar to those listed in the left column, while the response of series-SSHI is similar to those listed in the right column.

	Optimal operating points (Ω , r)	
	(Parallel-SSHI)	(Series-SSHI)
	$\Omega_{sc}^{opt} \sim \Omega_{sc} = 1$	$\Omega_{oc}^{opt} \sim \Omega_{oc} = \sqrt{1 + k_e^2}$
Optimal outputs	$r_{sc}^{opt} \propto \frac{1}{\frac{k_e^2}{\zeta_m}}$	$r_{oc}^{opt} \propto \frac{1}{(1+k_e^2)} \frac{k_e^2}{\zeta_m}$
Displacement	$\bar{u}_0^{opt} \propto \frac{1}{\zeta_m}$	$\bar{u}_0^{opt} \propto \frac{1}{\zeta_m(\sqrt{1+k_e^2})}$
Voltage	$\bar{V}_c^{opt} \propto 1$	$\bar{V}_c^{opt} \propto \frac{1}{\sqrt{1+k_e^2}} \frac{k_e^2}{\zeta_m}$
Current	$\bar{I}^{opt} \propto \frac{k_e^2}{\zeta_m}$	$\bar{I}^{opt} \propto \sqrt{1+k_e^2}$
Power	$\bar{P}^{opt} \propto \frac{1}{\zeta_m}$	$\bar{P}^{opt} \propto \frac{1}{\zeta_m}$

2.2. Series-SSHI Interface

Consider a series-SSHI interfacing circuit illustrated in figure 2(b). It consists of adding up a switching device in series with the piezoelectric structure. The electronic switch is triggered at the extreme values of displacement of the mass. Different from the case of the parallel-SSHI technique [12], the piezoelectric element is under an open circuit condition for most of the vibration time due to a quick inversion of the piezoelectric voltage operated by the switch. Therefore, the piezoelectric current I is always null except during the voltage inversion phases. The typical waveforms of displacement and piezoelectric voltage are provided in figure 3(b), where the displacement at the steady-state operation is

$$u(t) = u_0 \sin(\omega t - \theta), \quad (9)$$

with u_0 as the magnitude and θ as the phase shift. Guyomar *et al* [12] have performed the SSHI analysis assuming the in-phase assumption, i.e. the effect of the phase shift θ in equation (9) is insignificant. However, it has been shown that the in-phase estimates differ profoundly from the improved

estimates of the standard and parallel-SSHI systems if the electromechanical coupling of the system is not small [44, 46]. In addition, it is required to consider the phase-shift effect for estimating the reduction in power due to frequency deviation from resonance. Thus, such an effect has to be included in analyzing the electrical response of a series-SSHI system.

Now let t_i and t_f be two time instants such that the displacement $u(t)$ goes from the minimum $-u_0$ to the maximum u_0 , as demonstrated in figure 3(b). When the switch is on at time instant t_i , the piezoelectric voltage $V_p(t_i) = -V_M$ is reversed to $V_p(t_i^+) = V_m$ during the inversion. The inversion process can be understood by an electrically oscillating circuit consisting of the piezoelectric element in series with an inductance L at a battery-like rectified voltage V_c . This process is assumed to be quasi-instantaneous in the sense that the inversion time is chosen to be much smaller than the period of the mechanical vibration, i.e. $\Delta t = t_i^+ - t_i \approx \pi \sqrt{LC_p} \ll T$, where $T = \frac{2\pi}{\omega}$ [19]. As the rectified voltage V_c is almost kept constant due to large C_e , this gives $-(V_M - V_c) = -V_m - V_c$ in the ideal case. However, due to the electrical loss in the switching mechanism, the inversion is determined by

$$-(V_M - V_c)q_1 = -(V_M - V_c)e^{\frac{-\pi}{2Q_1}} = -V_m - V_c, \quad (10)$$

where Q_1 is the inversion quality factor and $q_1 = e^{\frac{-\pi}{2Q_1}}$.

Each time the switch turns on, the electric charge passing through the inductor L transmits a part of the energy stored in the piezoelectric capacitor C_p to the storage circuit. Therefore, the charge conservation is

$$C_p \Delta V = C_p(V_M + V_m) = \frac{T}{2} \frac{V_c}{R} = \frac{\pi}{\omega} \frac{V_c}{R}. \quad (11)$$

Next, from equation (2), we have

$$\int_{t_i^+}^{t_f} (-\Theta \dot{u} + C_p \dot{V}_p) dt = - \int_{t_i^+}^{t_f} I(t) dt = 0.$$

This results in

$$V_M - V_m = \frac{2\Theta}{C_p} u_0. \quad (12)$$

Combining equations (10)–(12) provides the relation between the magnitude of displacement and the rectified voltage:

$$V_c = \frac{2\Theta R w(1+q_1)}{\pi(1-q_1) + 2C_p R w(1+q_1)} u_0. \quad (13)$$

The estimation of harvested power can be found once the magnitude of displacement u_0 is determined due to equation (13). Next consider the balance of energy which is obtained by adding equation (1) multiplied by $\dot{u}(t)$ and equation (2) multiplied by $V_p(t)$. Integration of the energy balance equation from time t_i^+ to t_f gives energy conservation

$$\begin{aligned} \int_{t_i^+}^{t_f} F(t)\dot{u}(t) dt &= \int_{t_i^+}^{t_f} \eta_m \dot{u}^2(t) dt + \int_{t_i^+}^{t_f} V_p(t)I(t) dt \\ &+ \frac{1}{2} M \dot{u}^2(t)|_{t_i^+}^{t_f} + \frac{1}{2} K u^2(t)|_{t_i^+}^{t_f} + \frac{1}{2} C_p V_p^2(t)|_{t_i^+}^{t_f} \\ &= \int_{t_i^+}^{t_f} \eta_m \dot{u}^2(t) dt + \frac{1}{2} C_p (V_M^2 - V_m^2). \end{aligned} \quad (14)$$

Substituting equation (9) into equation (14) gives

$$\frac{\pi}{2} F_0 u_0 \sin \theta = \frac{\pi}{2} \eta_m w u_0^2 + \frac{T}{2} \frac{V_c^2}{R} + \frac{1}{2} C_p (1 - q_1^2) (V_M - V_c)^2, \quad (15)$$

where equations (10) and (11) are used for deriving equation (15). To eliminate the phase shift θ in equation (15), consider from equation (2)

$$\Theta \dot{V}_p(t) = \frac{\Theta}{C_p} [-I(t) + \Theta \dot{u}(t)]. \quad (16)$$

Substituting equation (16) into equation (1) by differentiating with respect to time t gives

$$M \frac{d}{dt} \ddot{u}(t) + \eta_m \frac{d}{dt} \dot{u}(t) + \left(K + \frac{\Theta^2}{C_p} \right) \frac{d}{dt} u(t) - \frac{\Theta}{C_p} I(t) = \frac{d}{dt} F(t). \quad (17)$$

Integrating equation (17) from t_i^+ to t_f provides

$$\left(K - M w^2 + \frac{\Theta^2}{C_p} \right) u_0 = F_0 \cos \theta. \quad (18)$$

The comparison between equations (15) and (18) eliminates the phase shift θ and gives the explicit form of displacement magnitude

$$u_0 = \frac{F_0}{\left\{ \left[\eta_m w + \frac{4\Theta^2(1+q_1)}{C_p [2C_p R w(1+q_1) + \pi(1-q_1)]} \right]^2 + \left(K - w^2 M + \frac{\Theta^2}{C_p} \right)^2 \right\}^{\frac{1}{2}}}.$$

The average harvested power is therefore obtained once u_0 is determined due to equation (13) and $P = \frac{V_c^2}{R}$. Finally, the displacement, voltage and harvested power in a series-SSHI system are expressed in terms of dimensionless parameters defined in equation (7) by

$$\begin{aligned} \bar{u}_0^{\text{Series-SSHI}} &= \frac{u_0^{\text{Series-SSHI}}}{\frac{F_0}{K}} \\ &= \frac{1}{\left\{ \left[2\zeta_m \Omega + \frac{4k_e^2(1+q_1)}{(1-q_1)\pi + 2r\Omega(1+q_1)} \right]^2 + (1 + k_e^2 - \Omega^2)^2 \right\}^{\frac{1}{2}}} \end{aligned} \quad (19)$$

$$\begin{aligned} \bar{V}_c^{\text{Series-SSHI}} &= \frac{V_c^{\text{Series-SSHI}}}{\frac{F_0}{\Theta}} = \frac{2r\Omega(1+q_1)}{(1-q_1)\pi + 2r\Omega(1+q_1)} \\ &\times \frac{k_e^2}{\left\{ \left[2\zeta_m \Omega + \frac{4k_e^2(1+q_1)}{(1-q_1)\pi + 2r\Omega(1+q_1)} \right]^2 + (1 + k_e^2 - \Omega^2)^2 \right\}^{\frac{1}{2}}}, \end{aligned} \quad (20)$$

$$\begin{aligned} \bar{P}^{\text{Series-SSHI}} &= \frac{P^{\text{Series-SSHI}}}{\frac{F_0^2}{\omega_{sc} M}} = \left\{ \frac{2(1+q_1)}{(1-q_1)\pi + 2r\Omega(1+q_1)} \right\}^2 \\ &\times \frac{k_e^2 \Omega^2 r}{\left\{ \left[2\zeta_m \Omega + \frac{4k_e^2(1+q_1)}{(1-q_1)\pi + 2r\Omega(1+q_1)} \right]^2 + (1 + k_e^2 - \Omega^2)^2 \right\}}. \end{aligned} \quad (21)$$

To further analyze the results given by equations (19)–(21), consider the case of ideal inversion, i.e. the inversion of the piezoelectric voltage V_p is complete so that $Q_1 = \infty$ and $q_1 = e^{\frac{\pi}{Q_1}} = 1$. Under this circumstance, the normalized harvested power becomes

$$\bar{P}^{\text{Series-SSHI}} = \frac{k_e^2 r}{\{4(\zeta_m r + \frac{k_e^2}{\Omega^2})^2 \Omega^2 + (1 + k_e^2 - \Omega^2)^2 r^2\}}. \quad (22)$$

The optimal operation point occurs at the open circuit resonance Ω_{oc} and the corresponding optimal electrical load resistance and harvested power are therefore

$$r_{\text{series}}^{\text{opt}} = \left(\frac{1}{1 + k_e^2} \right) \frac{k_e^2}{\zeta_m}, \quad \bar{P}^{\text{Series-SSHI}}|_{r=r^{\text{opt}}, \Omega=\Omega_{oc}} = \frac{1}{16\zeta_m}. \quad (23)$$

From equation (23), the optimal load resistance is proportional to the ratio $\frac{k_e^2}{\zeta_m}$, while the corresponding optimal power depends only on the mechanical damping ratio ζ_m and is independent of the electromechanical coupling coefficient k_e^2 . Comparing all of these features with the right column of table 1 suggests that the behavior of the power harvesting system using the series-SSHI interface is similar to that of the strongly coupled electromechanical standard system operated at the open circuit resonance Ω_{oc} .

In addition, the harvested average power based on the series-SSHI technique always achieves the saturation value $\frac{1}{16\zeta_m}$ no matter whether the real system is weakly or strongly electromechanically coupled. To see it, figure 4(b) shows power extraction against electrical load and applied frequency for an ideal series-SSHI system with weak electromechanical coupling ($k_e^2 = 0.01$, $\zeta_m = 0.03$, $\frac{k_e^2}{\zeta_m} = 0.33$). The peak of power is identical to that of a strongly electromechanically coupled system using the standard interface ($k_e^2 = 1.0$, $\zeta_m = 0.03$, $\frac{k_e^2}{\zeta_m} = 33$). Thus, power extraction is obviously enhanced for a weakly coupled electromechanical system using the series-SSHI electronic interface.

2.3. Parallel-SSHI interface

Figure 2(c) shows another version of SSHI interface, called parallel-SSHI. It consists of adding up a switching device in parallel with the piezoelectric structure. The electronic switch is triggered according to the maximum and minimum of the

displacement of the mass. As a result, this gives an inversion of the piezoelectric voltage V_p at each extremum, i.e. V_p is changed either from $-V_c$ to $q_1 V_c$ or from V_c to $-q_1 V_c$, as illustrated in figure 3(c). Here $q_1 = e^{\frac{-\pi}{2Q_1}}$ and Q_1 is the inversion quality factor due to the energy loss mainly from the inductor in series with the switch. Different from the in-phase analysis [12], Shu *et al* have provided an improved analysis taking into account the effect of phase shift and shown (see equations (6)–(8) in [46])

$$\bar{u}_0^{\text{Para-SSHI}} = \frac{u_0^{\text{Para-SSHI}}}{\frac{F_0}{K}} = \frac{1}{\left\{ \left(2\zeta_m + \frac{2(1+\frac{r\Omega}{2})(1-q_1^2)k_c^2 r}{(\frac{1-q_1}{2}r\Omega + \frac{\pi}{2})^2} \right)^2 \Omega^2 + \left(1 - \Omega^2 + \frac{(\frac{1-q_1}{2}k_c^2 r\Omega}{(\frac{1-q_1}{2}r\Omega + \frac{\pi}{2})} \right)^2 \right\}^{\frac{1}{2}}}, \quad (24)$$

$$\bar{V}_c^{\text{Para-SSHI}} = \frac{V_c^{\text{Para-SSHI}}}{\frac{F_0}{\Theta}} = \left(\frac{r\Omega}{(\frac{1-q_1}{2}r\Omega + \frac{\pi}{2})} \right) \frac{k_c^2}{\left\{ \left(2\zeta_m + \frac{2(1+\frac{r\Omega}{2})(1-q_1^2)k_c^2 r}{(\frac{1-q_1}{2}r\Omega + \frac{\pi}{2})^2} \right)^2 \Omega^2 + \left(1 - \Omega^2 + \frac{(\frac{1-q_1}{2}k_c^2 r\Omega}{(\frac{1-q_1}{2}r\Omega + \frac{\pi}{2})} \right)^2 \right\}^{\frac{1}{2}}}, \quad (25)$$

$$\bar{P}^{\text{Para-SSHI}} = \frac{P^{\text{Para-SSHI}}}{\frac{F_0^2}{w_{sc}M}} = \frac{1}{\left(\frac{1-q_1}{2}r\Omega + \frac{\pi}{2} \right)^2} \frac{k_c^2 \Omega^2 r}{\left\{ \left(2\zeta_m + \frac{2(1+\frac{r\Omega}{2})(1-q_1^2)k_c^2 r}{(\frac{1-q_1}{2}r\Omega + \frac{\pi}{2})^2} \right)^2 \Omega^2 + \left(1 - \Omega^2 + \frac{(\frac{1-q_1}{2}k_c^2 r\Omega}{(\frac{1-q_1}{2}r\Omega + \frac{\pi}{2})} \right)^2 \right\}}. \quad (26)$$

These results given by equations (24)–(26) can be interpreted by considering the case where the inversion of the piezoelectric voltage V_p is complete, i.e. $Q_1 = \infty$. This gives $q_1 = 1$ and the normalized harvested power becomes

$$\bar{P}^{\text{Para-SSHI}} = \frac{4}{\pi^2} \frac{k_c^2 \Omega^2 r}{4(\zeta_m + \frac{4k_c^2 r}{\pi^2})^2 \Omega^2 + (1 - \Omega^2)^2}. \quad (27)$$

The optimal electric load resistance and the normalized power operated at Ω_{sc} are therefore

$$r_{\text{para}}^{\text{opt}} = \frac{\pi^2}{4} \frac{1}{\frac{k_c^2}{\zeta_m}}, \quad \bar{P}^{\text{Para-SSHI}}|_{r=r^{\text{opt}}, \Omega=\Omega_{sc}} = \frac{1}{16\zeta_m}. \quad (28)$$

In contrast to the case of series-SSHI, equation (28) indicates that the optimal load resistance is inversely proportional to the ratio $\frac{k_c^2}{\zeta_m}$. The corresponding optimal power is, however, identical to that of the series-SSHI case. It depends only on the mechanical damping ratio ζ_m and is independent of the electromechanical coupling coefficient k_c^2 . Moreover, comparing all of these features with the left column of table 1 suggests that the behavior of a parallel-SSHI system is similar to that of the strongly coupled electromechanical standard system operated at the short circuit resonance Ω_{sc} . As this result is valid even when the real electromechanical system is weakly coupled, the harvested power is increased significantly when compared to the standard system. For example, figure 4(c) shows harvested power of an ideal

parallel-SSHI system with weak electromechanical coupling ($k_c^2 = 0.01$, $\zeta_m = 0.03$, $\frac{k_c^2}{\zeta_m} = 0.33$). The peak power is enhanced to be identical to that of a strongly coupled electromechanical standard system ($k_c^2 = 1$, $\zeta_m = 0.03$, $\frac{k_c^2}{\zeta_m} = 0.33$) shown in figure 4(a).

3. Results

3.1. Validation

The validation of the proposed improved estimates is carried out numerically by transforming equations (1)–(3) to an equivalent circuit system with $R^* = \frac{\eta_m}{\Theta^2}$ as resistance, $L^* = \frac{M}{\Theta^2}$ as inductance, $C^* = \frac{\Theta^2}{K}$ as capacitance and $V_{\text{source}} = \frac{F_0}{\Theta}$ as the voltage source, as shown in figure 5(a). The equivalent circuit is endowed with a series-SSHI electronic interface with the quality factor of voltage inversion $Q_1 = 3.5$ [12]. The common software PSpice, which is based on the SPICE (Simulation Program with Integrated Circuit Emphasis) algorithms, is adopted for circuit simulation. The simulation parameters are $R^* = 66870 \Omega$, $L^* = 2051 \text{ H}$, $C^* = 0.7338 \text{ nF}$, $V_{\text{source}} = 4.833 \text{ V}$ and $C_p = 9.718 \text{ nF}$. This gives the system parameters $k_c^2 = 0.0755$ and $\zeta_m = 0.02$. The results are demonstrated in figure 5(b) where the normalized power from equation (21) is plotted against the frequency ratio evaluated at the optimal load $r^{\text{opt}} = 3.84$. The in-phase estimates [2, 21] are also provided here for comparison and are denoted by dashed lines. The analytical estimates and numerical simulations are represented by solid lines and open circles in figure 5(b). Obviously, the numerical simulations are favorable to the results predicted based on the proposed improved estimates, since the in-phase estimates lack frequency dependence. In addition, other parameters are also chosen and the results show similar contrasting comparisons between the in-phase and improved estimates. Thus, the in-phase estimates are unable to predict the system behavior if the driving frequency deviates from the resonance frequency. The proposed improved estimates are therefore suitable for the performance evaluation of the electrical behavior of a series-SSHI system.

3.2. Comparison

Table 1 highlights the striking contrast in the behaviors of ideal parallel- and series-SSHI systems ($Q_1 = \infty$). However, the inversion of the piezoelectric voltage due to electrical oscillation by an inductor is typically not perfect ($Q_1 \neq \infty$). This gives a certain amount of performance degradation using the SSHI techniques. In addition, the harvested average power crucially depends on the different magnitudes of the ratio of the electromechanical coupling coefficient to the mechanical damping ratio, i.e. $\frac{k_c^2}{\zeta_m}$. Thus, these factors have to be taken into account in comparing these different techniques. Assume $Q_1 = 4.4$. A much larger value of quality factor Q_1 can be obtained by requiring the use of the low loss inductor.

First consider the case of a weakly coupled electromechanical system, i.e. the ratio $\frac{k_c^2}{\zeta_m} \ll 1$. We take $k_c = 0.1$

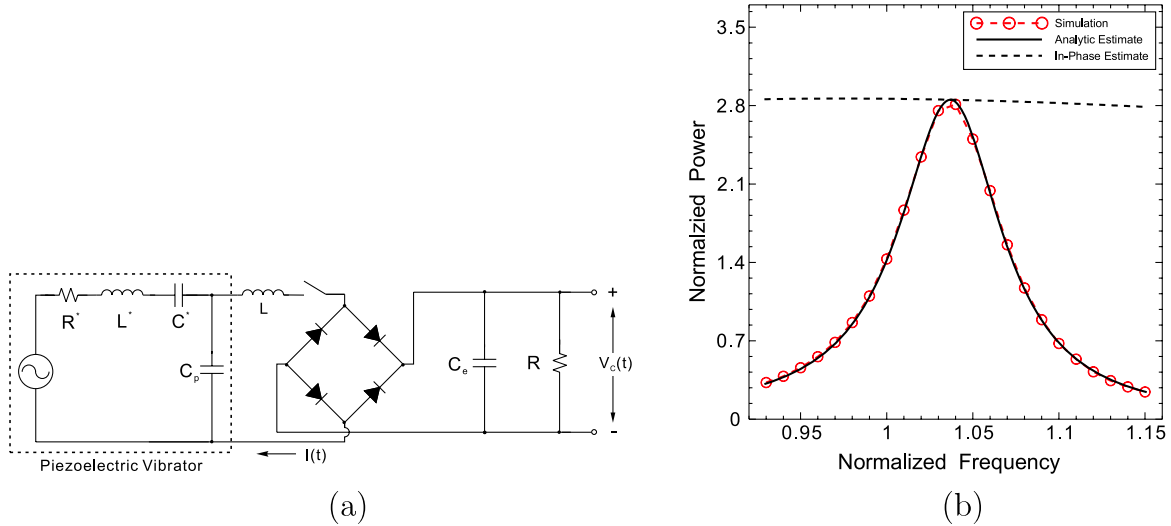


Figure 5. Numerical validation of the proposed analytical estimates of harvested power in a series-SSHI system with parameters $k_c^2 = 0.0755$, $\zeta_m = 0.02$, $\frac{k_e^2}{\zeta_m} = 3.77$ and $Q_1 = 3.5$. (a) The equivalent circuit model for the piezoelectric device endowed with a series-SSHI electronic interface. (b) The numerical simulation results are compared with those predicted by analytical and in-phase estimates.

Table 2. Optimal power achieved at different operating points are compared for parallel-SSHI/standard/series-SSHI interfaces under various magnitudes of electromechanical coupling to mechanical damping: weak coupling ($\frac{k_e^2}{\zeta_m} = 0.3$), medium coupling ($\frac{k_e^2}{\zeta_m} = 3.0$) and strong coupling ($\frac{k_e^2}{\zeta_m} = 33.3$).

Optimal conditions	Parallel-SSHI (Ω_{sc})		Standard ($\Omega_{sc} < \Omega < \Omega_{oc}$)		Series-SSHI (Ω_{oc})	
	Power	Load	Power	Load	Power	Load
Weak coupling	—	—	0.4	1.55	—	—
$Q_1 = \infty$	2.1	7.4	—	—	2.1	0.33
$Q_1 = 4.4$	1.2	4.62	—	—	1.1	0.61
Medium coupling	—	—	1.8	1.51	—	—
$Q_1 = \infty$	2.1	0.82	—	—	2.1	2.75
$Q_1 = 4.4$	1.9	0.78	—	—	1.9	3.02
Strong coupling	—	—	2.1	0.08 (Ω_{sc}) / 16.2 (Ω_{oc})	—	—
$Q_1 = \infty$	2.1	0.074	—	—	2.1	16.67
$Q_1 = 4.4$	2.1	0.07	—	—	2.1	17.0

and $\zeta_m = 0.03$ for demonstration. This gives $\frac{k_e^2}{\zeta_m} = 0.33$. The harvested power versus frequency ratio for various normalized resistances are shown in figure 6(a) based on the parallel-SSHI interface, in figure 6(d) based on the standard interface and in figure 6(g) based on the series-SSHI. The maximum normalized power generated for the ideal voltage inversion is around $\bar{P}^{\text{Para-SSHI}}|_{Q_1=\infty} = 2.1$ at $\Omega = \Omega_{sc}$ and $r = 7.4$ for parallel-SSHI, while it is $\bar{P}^{\text{Series-SSHI}}|_{Q_1=\infty} = 2.1$ at $\Omega = \Omega_{oc}$ and $r = 0.33$ for series-SSHI. However, both are reduced to $\bar{P}^{\text{Para-SSHI}}|_{Q_1=4.4} = 1.2$ and $\bar{P}^{\text{Series-SSHI}}|_{Q_1=4.4} = 1.1$ in the non-ideal voltage inversion. While the harvested power based on the SSHI techniques is three times larger than that using the standard interface ($\bar{P}^{\text{Standard}} = 0.4$), the performance degradation is significant for both parallel- and series-SSHI. The detailed operating points for generating the peak power are listed in table 2.

Next, suppose the electromechanical coupling is in the medium range, i.e. the ratio of $\frac{k_e^2}{\zeta_m}$ is of the order of one. We take $k_e = 0.3$ and $\zeta_m = 0.03$. This gives $\frac{k_e^2}{\zeta_m} = 3$. The harvested power versus frequency ratio for

various normalized resistances are shown in figure 6(b) based on the parallel-SSHI interface, in figure 6(e) based on the standard interface, and in figure 6(h) based on the series-SSHI interface. Different from the previous case of weak coupling, the reduction in power is not significant in this case. Indeed, the maximum normalized power for the non-ideal voltage inversion is $\bar{P}^{\text{Parallel-SSHI}}|_{Q_1=4.4} = 1.9$ at $\Omega = \Omega_{sc}$ and $r = 0.78$ and $\bar{P}^{\text{Series-SSHI}}|_{Q_1=4.4} = 1.9$ at $\Omega = \Omega_{oc}$ and $r = 3.02$. Both are smaller than the ideal SSHI power ($\bar{P}^{\text{Para-SSHI}}|_{Q_1=\infty} = \bar{P}^{\text{Series-SSHI}}|_{Q_1=\infty} = 2.1$), but are slightly larger than that ($\bar{P}^{\text{Standard}} = 1.8$) using the standard electronic interface. The detailed operating points for achieving the peak power are listed in table 2.

In spite of no significant increase of power extraction using either the parallel-SSHI or series-SSHI electronic interfaces for the case of medium coupling, figures 6(b) or (h) demonstrate that the harvested power evaluated at around the optimal load is less sensitive to frequency deviation. Indeed, consider the standard case whose optimal power is achieved at around $r = \frac{\pi}{2}$. From figure 6(e), it is clear that there is a 57% power reduction for around 5% frequency deviation from the

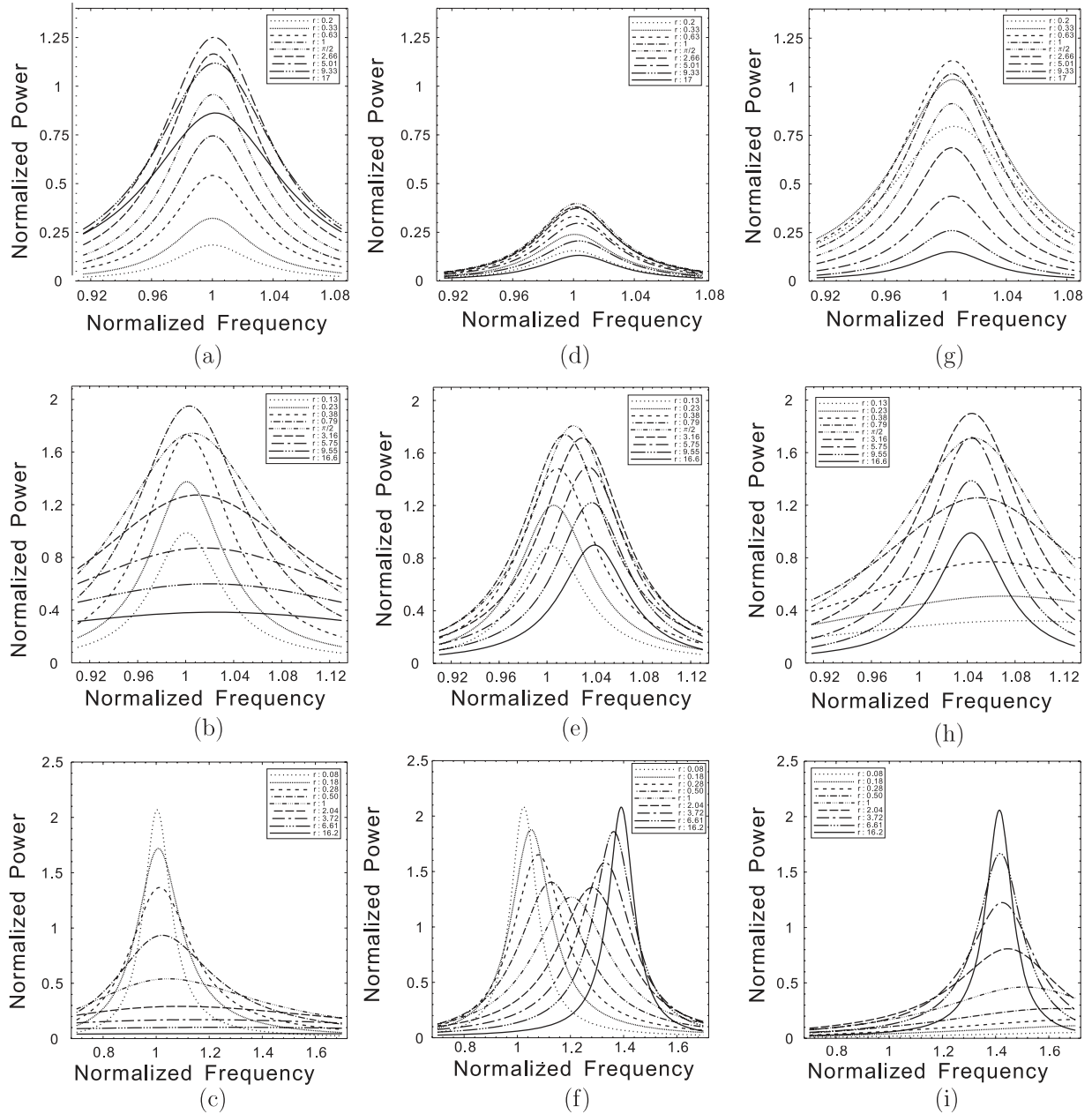


Figure 6. Normalized power versus frequency ratio for different values of normalized resistance. Notice that (a)–(c) are obtained using the parallel-SSHI electronic interface with different magnitudes of $\frac{k_e^2}{\zeta_m} = 0.3, 3.0, 33.3$, respectively; (d)–(f) are obtained using the standard electronic interface with different magnitudes of $\frac{k_e^2}{\zeta_m} = 0.3, 3.0, 33.3$, respectively; and (g)–(i) are obtained using the series-SSHI electronic interface with different magnitudes of $\frac{k_e^2}{\zeta_m} = 0.3, 3.0, 33.3$, respectively.

optimal frequency. In contrast to the standard case, figure 6(b) shows that the power reduction is around 30% for the same frequency deviation in the case of parallel-SSHI evaluated at the same electrical load ($r = \frac{\pi}{2}$). Similarly, the reduction in power is around 29% in the case of series-SSHI, as can be seen in figure 6(h) at $r = \frac{\pi}{2}$. In addition, it can be shown that this frequency-insensitive feature or wideband effect is much more pronounced if the quality factor of voltage inversion is further improved.

The last case is to discuss the electrical behavior of a strongly coupled electromechanical system ($\frac{k_e^2}{\zeta_m} \gg 1$). We

then take $k_e = 1$ and $\zeta_m = 0.03$, and this gives $\frac{k_e^2}{\zeta_m} = 33.3$. The harvested power versus frequency ratio for various normalized resistances are shown in figure 6(c) based on the parallel-SSHI interface, in figure 6(f) based on the standard interface, and in figure 6(i) based on the series-SSHI interface. As described in section 2.1, there are two identical peaks of optimal power in the standard case, while there is only one peak of power in either the parallel-SSHI or series-SSHI. Different from the cases of weak or medium coupling, there is no degradation in power as listed in table 2. A further investigation shows that the curve of peak power in the case of

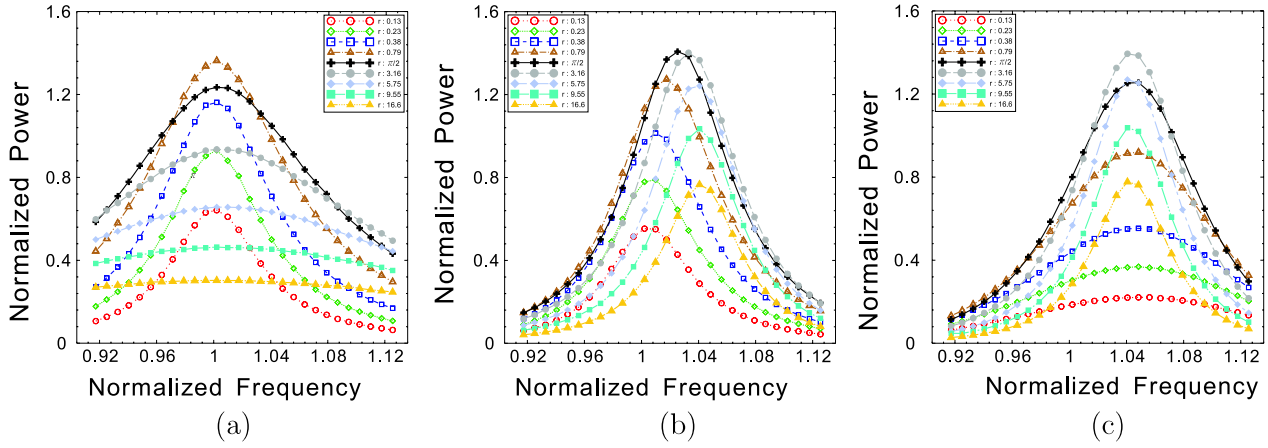


Figure 7. The effect of diode loss on the bandwidth improvement for (a) the parallel-SSHI, (b) the standard and (c) the series-SSHI systems ($k_c = 0.3$, $\zeta_m = 0.03$, $\frac{k_c^2}{\zeta_m} = 3$, $Q_1 = 4.4$).

parallel-SSHI is identical to that in the standard case operated at Ω_{sc} and $r = 0.08$. Similarly, the curve of peak power in the case of series-SSHI is identical to that in the standard case operated at Ω_{oc} and $r = 16.2$. Thus, from the point of view of deviations in frequencies or electrical loads, there seems to be no obvious advantages using either the parallel- or series-SSHI techniques for piezoelectric systems with strong electromechanical coupling.

3.3. Discussion

One of the important conclusions drawn from figure 6 is that both parallel- and series-SSHI systems show significant bandwidth improvement in the case of medium electromechanical coupling. But the effect of diode loss, which is inevitable in practical circuit systems, is not considered in figure 6, and therefore it is discussed here. Using the same system parameters of medium coupling as in figures 6(b), (e) and (h) and the PSpice equivalent circuit simulation, figure 7, accounting for the effect of diode loss shows a different electrical response between these two SSHI systems. To see it, consider the black line shown in figure 7(b). It represents the optimal power achieved at the normalized load $r = \frac{\pi}{2}$ in the standard case and it exhibits small bandwidth as expected. At the same normalized load as shown in the black lines of figures 7(a) and (c), the parallel-SSHI system shows around 19% power reduction for 5% frequency deviation, while the series-SSHI system exhibits 48% reduction in power. Thus, the feature of frequency insensitivity to power reduction is almost lost in the series-SSHI system, while it still remains in the parallel-SSHI system.

To explain the loss of wideband effect in series-SSHI systems, consider equations (27) and (22) representing the ideal harvested power in parallel-/series-SSHI systems, respectively. They are particular chosen since their mathematical expressions are simple for carrying out analysis. The sensibility of power reduction to frequency deviation can be realized by taking the derivatives of equations (27) and (22) with respect to frequency evaluated at around the optimal frequency and electrical load. Indeed, it can be shown that the

slope of power to frequency ratio in the parallel-SSHI system is approximated to

$$\frac{d\bar{P}^{\text{Para-SSHI}}}{d\Omega} = \frac{d\bar{P}^{\text{Para-SSHI}}}{df} \approx \frac{(1 + \chi)}{2(2 + \chi)^4 \zeta_m^3} \left\{ \frac{-f}{(1 + 2f)^2} \right\}, \quad (29)$$

where f and χ denote the amount of deviations in frequency and optimal electrical load and are defined by

$$\Omega = \Omega_{sc} + f, \quad r = r_{\text{para}}^{\text{opt}}(1 + \chi) = \frac{\pi^2}{4} \frac{k_c^2}{\zeta_m} (1 + \chi). \quad (30)$$

Thus, from equation (29), at the fixed frequency deviation f

$$\left| \frac{d\bar{P}^{\text{Para-SSHI}}}{d\Omega} \right|_{r > r_{\text{para}}^{\text{opt}}(\chi > 0)} < \left| \frac{d\bar{P}^{\text{Para-SSHI}}}{d\Omega} \right|_{r < r_{\text{para}}^{\text{opt}}(\chi < 0)}. \quad (31)$$

This result shows that power reduction in a parallel-SSHI system is less sensitive to frequency deviations if the terminal electrical loads are chosen to be slightly greater than the optimal load. Next, applying the similar analysis to the series-SSHI case gives

$$\frac{d\bar{P}^{\text{Series-SSHI}}}{d\Omega} = \frac{d\bar{P}^{\text{Series-SSHI}}}{df} \approx \frac{(1 + k_c^2)(1 + \chi)^3}{2\zeta_m^3(2 + \chi)^4} \left\{ \frac{-f}{(\sqrt{1 + k_c^2} + 2f)^2} \right\}, \quad (32)$$

where the derivations in frequency f and electrical load χ are defined by

$$\Omega = \Omega_{oc} + f, \quad r = r_{\text{series}}^{\text{opt}}(1 + \chi) = \frac{1}{1 + k_c^2} \frac{k_c^2}{\zeta_m} (1 + \chi). \quad (33)$$

Thus, at the fixed frequency deviation f , it can be shown easily that

$$\left| \frac{d\bar{P}^{\text{Series-SSHI}}}{d\Omega} \right|_{r < r_{\text{series}}^{\text{opt}}(\chi < 0)} < \left| \frac{d\bar{P}^{\text{Series-SSHI}}}{d\Omega} \right|_{r > r_{\text{series}}^{\text{opt}}(\chi > 0)}. \quad (34)$$

In contrast to the behavior of a parallel-SSHI system, the harvested power in an ideal series-SSHI system reduces insignificantly to frequency deviations at the loads slightly lower than its optimal load. Thus, the additional equivalent resistive load added to the system due to the consideration of diode loss results in distinct electrical response in these two SSHI cases. The improvement in bandwidth is basically lost in a series-SSHI system since such an effect occurs at loads slightly smaller than its optimal load.

4. Conclusion

An improved analysis accounting for the full electromechanical response and vibration phase-shift effect is proposed to investigate the electrical behavior of a piezoelectric energy harvester embedded with a series-SSHI electronic interface. The analytical expression of harvested power is provided and validated numerically. The performance evaluation of a series-SSHI system is carried out and compared with the piezoelectric systems using the standard or parallel-SSHI interfacing circuits. The results show that the electrical response of an ideal series-SSHI system is in sharp contrast to that of an ideal parallel-SSHI system. Indeed, no matter what the strength of electromechanical coupling of a real system is, a series-SSHI (parallel-SSHI) system is similar to the response of a strongly coupled electromechanical standard system operated at the open (short) circuit resonance. As a result, both can significantly boost the harvested power of weakly coupled electromechanical systems, except that the optimal electrical load of the former is proportional to the ratio of the coupling factor to mechanical damping, while it is inversely proportional to this ratio in the latter case, as summarized in table 1.

The performance degradation due to non-ideal voltage inversion is discussed and classified according to the relative strength of electromechanical coupling to mechanical damping, as illustrated in figure 6. A series-SSHI system shows the significant degradation in performance in a weakly coupled electromechanical system and no obvious advantages over the standard system with strong electromechanical coupling. However, similar to the behavior of a parallel-SSHI system, a series-SSHI system avails against the standard technique in the case of medium coupling. It shows that the peak power is close to the ideal optimal value and the power reduction is less sensitive to frequency deviation. Finally, the further analysis reveals that these two SSHI systems exhibit dissimilar electrical responses in harvested power if the effect of diode loss is considered. It turns out that the ability of bandwidth improvement might be lost in series-SSHI systems whereas it still remains in parallel-SSHI systems, as demonstrated in figure 7.

Acknowledgments

The support from the NSC under grant nos. 96-2628-E-002-119-MY3 and 99-2221-E-002-071-MY3 is appreciated.

References

- [1] Ajitsaria J, Choe S Y, Shen D and Kim D J 2007 Modeling and analysis of a bimorph piezoelectric cantilever beam for voltage generation *Smart Mater. Struct.* **16** 447–54
- [2] Badel A, Benayad A, Lefeuvre E, Lebrun L, Richard C and Guyomar D 2006 Single crystals and nonlinear process for outstanding vibration-powered electrical generators *IEEE Trans. Ultrason. Ferroelectr. Freq. Control* **53** 673–84
- [3] Cottone F, Vocca H and Gammaitoni L 2009 Nonlinear energy harvesting *Phys. Rev. Lett.* **102** 080601
- [4] Dietl J M, Wickenheiser A M and Garcia E 2010 A timoshenko beam model for cantilevered piezoelectric energy harvesters *Smart Mater. Struct.* **19** 055018
- [5] duToit N E, Wardle B L and Kim S G 2005 Design considerations for MEMS-scale piezoelectric mechanical vibration energy harvesters *Integr. Ferroelectr.* **71** 121–60
- [6] Elvin N G and Elvin A A 2009 A coupled finite element circuit simulation model for analyzing piezoelectric energy generators *J. Intell. Mater. Syst. Struct.* **20** 587–95
- [7] Elvin N G, Lajnef N and Elvin A A 2006 Feasibility of structural monitoring with vibration powered sensors *Smart Mater. Struct.* **15** 977–86
- [8] Erturk A and Inman D J 2008 Issues in mathematical modeling of piezoelectric energy harvesters *Smart Mater. Struct.* **17** 065016
- [9] Erturk A and Inman D J 2009 An experimentally validated bimorph cantilever model for piezoelectric energy harvesting from base excitations *Smart Mater. Struct.* **18** 025009
- [10] Guan M J and Liao W H 2007 On the efficiencies of piezoelectric energy harvesting circuits towards storage device voltages *Smart Mater. Struct.* **16** 498–505
- [11] Guan M J and Liao W H 2008 Characteristics of energy storage devices in piezoelectric energy harvesting systems *J. Intell. Mater. Syst. Struct.* **19** 671–80
- [12] Guyomar D, Badel A, Lefeuvre E and Richard C 2005 Toward energy harvesting using active materials and conversion improvement by nonlinear processing *IEEE Trans. Ultrason. Ferroelectr. Freq. Control* **52** 584–95
- [13] Hu H P, Cui Z J and Cao J G 2007 Performance of a piezoelectric bimorph harvester with variable width *J. Mech.* **23** 197–202
- [14] Hu Y T, Hu T and Jiang Q 2008 On the interaction between the harvesting structure and the storage circuit of a piezoelectric energy harvester *Int. J. Appl. Electromagn. Mech.* **27** 297–309
- [15] Jeon Y B, Sood R, Jeong J H and Kim S G 2005 MEMS power generator with transverse mode thin film PZT *Sensors Actuators A* **122** 16–22
- [16] Jiang S, Li X, Guo S, Hu Y, Yang J and Jiang Q 2005 Performance of a piezoelectric bimorph for scavenging vibration energy *Smart Mater. Struct.* **14** 769–74
- [17] Kauffman J L and Lesieutre G A 2009 A low-order model for the design of piezoelectric energy harvesting devices *J. Intell. Mater. Syst. Struct.* **20** 495–504
- [18] Kim S, Clark W W and Wang Q M 2005 Piezoelectric energy harvesting with a clamped-circular plate: analysis *J. Intell. Mater. Syst. Struct.* **16** 847–54
- [19] Lallart M and Guyomar D 2008 An optimized self-powered switching circuit for non-linear energy harvesting with low voltage output *Smart Mater. Struct.* **17** 035030
- [20] Lee B S, Lin S C, Wu W J, Wang X Y, Chang P Z and Lee C K 2009 Piezoelectric MEMS generators fabricated with an aerosol deposition PZT thin film *J. Micromech. Microeng.* **19** 065014
- [21] Lefeuvre E, Badel A, Richard C, Petit L and Guyomar D 2006 A comparison between several vibration-powered piezoelectric generators for standalone systems *Sensors Actuators A* **126** 405–16

- [22] Lesieutre G A, Ottman G K and Hofmann H F 2004 Damping as a result of piezoelectric energy harvesting *J. Sound Vib.* **269** 991–1001
- [23] Liang J R and Liao W H 2009 Piezoelectric energy harvesting and dissipation on structural damping *J. Intell. Mater. Syst. Struct.* **20** 515–27
- [24] Liao Y and Sodano H A 2008 Model of a single mode energy harvester and properties for optimal power generation *Smart Mater. Struct.* **17** 065026
- [25] Liao Y and Sodano H A 2009 Optimal parameters and power characteristics of piezoelectric energy harvesters with an RC circuit *Smart Mater. Struct.* **18** 045011
- [26] Lin H R, Chen C S, Chen P Y, Tsai F J, Huang J D, Li J F, Lin C T and Wu W J 2010 Design of wireless sensor network and its application for structure health monitoring of cable-stayed bridge *Smart Struct. Syst.* at press
- [27] Liu Y, Tian G, Wang Y, Lin J, Zhang Q and Hofmann H F 2009 Active piezoelectric energy harvesting: general principle and experimental demonstration *J. Intell. Mater. Syst. Struct.* **20** 575–85
- [28] Majdoub M S, Sharma P and Cagin T 2008 Enhanced size-dependent piezoelectricity and elasticity in nanostructures due to the flexoelectric effect *Phys. Rev. B* **77** 125424
- [29] Makihara K, Onoda J and Miyakawa T 2006 Low energy dissipation electric circuit for energy harvesting *Smart Mater. Struct.* **15** 1493–8
- [30] Mathers A, Moon K S and Yi J 2009 A vibration-based PMN-PT energy harvester *IEEE Sensors J.* **9** 731–9
- [31] Mitcheson P D, Yeatman E M, Rao G K, Holmes A S and Green T C 2008 Energy harvesting from human and machine motion for wireless electronic devices *Proc. IEEE* **96** 1457–86
- [32] Mo C, Radziemski L J and Clark W W 2010 Analysis of piezoelectric circular diaphragm energy harvesters for use in a pressure fluctuating system *Smart Mater. Struct.* **19** 025016
- [33] Ottman G K, Hofmann H F, Bhatt A C and Lesieutre G A 2002 Adaptive piezoelectric energy harvesting circuit for wireless remote power supply *IEEE Trans. Power Electron.* **17** 669–76
- [34] Ottman G K, Hofmann H F and Lesieutre G A 2003 Optimized piezoelectric energy harvesting circuit using step-down converter in discontinuous conduction mode *IEEE Trans. Power Electron.* **18** 696–703
- [35] Paquin S and St-Amant Y 2010 Improving the performance of a piezoelectric energy harvester using a variable thickness beam *Smart Mater. Struct.* **19** 105020
- [36] Poulin G, Sarraute E and Costa F 2004 Generation of electric energy for portable devices: comparative study of an electromagnetic and a piezoelectric system *Sensors Actuators A* **116** 461–71
- [37] Priya S 2005 Modeling of electric energy harvesting using piezoelectric windmill *Appl. Phys. Lett.* **87** 184101
- [38] Qin Y, Wang X and Wang Z L 2008 Microfibre-nanowire hybrid structure for energy scavenging *Nature* **451** 809–U5
- [39] Richards C D, Anderson M J, Bahr D F and Richards R F 2004 Efficiency of energy conversion for devices containing a piezoelectric component *J. Micromech. Microeng.* **14** 717–21
- [40] Roundy S, Wright P K and Rabaey J 2003 A study of low level vibrations as power source for wireless sensor nodes *Comput. Commun.* **26** 1131–44
- [41] Rupp C J, Evgrafov A, Maute K and Dunn M L 2009 Design of piezoelectric energy harvesting systems: a topology optimization approach based on multilayer plates and shells *J. Intell. Mater. Syst. Struct.* **20** 1923–39
- [42] Scruggs J T 2009 An optimal stochastic control theory for distributed energy harvesting networks *J. Sound Vib.* **320** 707–25
- [43] Seuaciuc-Osorio T and Daqaq M F 2009 On the reduced-order modeling of energy harvesters *J. Intell. Mater. Syst. Struct.* **20** 2003–16
- [44] Shu Y C and Lien I C 2006 Analysis of power output for piezoelectric energy harvesting systems *Smart Mater. Struct.* **15** 1499–512
- [45] Shu Y C and Lien I C 2006 Efficiency of energy conversion for a piezoelectric power harvesting system *J. Micromech. Microeng.* **16** 2429–38
- [46] Shu Y C, Lien I C and Wu W J 2007 An improved analysis of the SSHI interface in piezoelectric energy harvesting *Smart Mater. Struct.* **16** 2253–64
- [47] Shu Y C, Lien I C, Wu W J and Shiu S M 2009 Comparisons between parallel- and series-SSHI interfaces adopted by piezoelectric energy harvesting systems *Active and Passive Smart Structures and Integrated Systems; Proc. SPIE* **7288** 728808
- [48] Sodano H A, Inman D J and Park G 2004 A review of power harvesting from vibration using piezoelectric materials *Shock Vib. Dig.* **36** 197–205
- [49] Song H J, Choi Y T, Purekar A S and Wereley N M 2009 Performance evaluation of multi-tier energy harvesters using macro-fiber composite patches *J. Intell. Mater. Syst. Struct.* **20** 2077–88
- [50] Sun C, Qin L, Li F and Wang Q M 2009 Piezoelectric energy harvesting using single crystal $\text{Pb}(\text{Mg}_{1/3}\text{Nb}_{2/3})\text{O}_{3-x}\text{PbTiO}_3$ (PMN-PT) device *J. Intell. Mater. Syst. Struct.* **20** 559–68
- [51] Wang Q M and Cross L E 1999 Constitutive equations of symmetrical triple layer piezoelectric benders *IEEE Trans. Ultrason. Ferroelectr. Freq. Control* **46** 1343–51
- [52] Wickenheiser A M and Garcia E 2010 Broadband vibration-based energy harvesting improvement through frequency up-conversion by magnetic excitation *Smart Mater. Struct.* **19** 065020
- [53] Wickenheiser A M, Reissman T, Wu W J and Garcia E 2010 Modeling the effects of electromechanical coupling on energy storage through piezoelectric energy harvesting *IEEE/ASME Trans. Mechatronics* **15** 400–11
- [54] Wu W J, Wickenheiser A M, Reissman T and Garcia E 2009 Modeling and experimental verification of synchronized discharging techniques for boosting power harvesting from piezoelectric transducers *Smart Mater. Struct.* **18** 055012
- [55] Yang Y and Tang L 2009 Equivalent circuit modeling of piezoelectric energy harvesters *J. Intell. Mater. Syst. Struct.* **20** 2223–35
- [56] Yang Z and Yang J 2009 Connected vibrating piezoelectric bimorph beams as a wide-band piezoelectric power harvester *J. Intell. Mater. Syst. Struct.* **20** 569–74